High performance metallic joints from screen-printed Cu@Ag nanopastes

Thomas Michaud, Thierry Baffie, Sonia Sousa Nobre, Jean-Michel Missiaen, Didier Bouvard, Jean-Pierre Simonato

High performance metallic joints from screen-printed Cu@Ag nanopastes

Thomas Michaud [a], Thierry Baffie [a*], Sonia Sousa Nobre [a], Jean-Michel Missiaen [b], Didier Bouvard [b] and Jean-Pierre Simonato [a,c*]

[a] Univ. Grenoble Alpes, CEA, LITEN DTNM, 38054 Grenoble, France.
[b] Univ. Grenoble Alpes, CNRS, Grenoble INP, SIMAP, 38000, Grenoble, France
[c] Duke University, Department of Chemistry, 124 Science Drive, Durham, NC 27708, USA

* Corresponding authors

E-mail: thierry.baffie@cea.fr; jean-pierre.simonato@cea.fr

Keywords: Metallic joint; power electronics; core-shell nanoparticles; dilatometry; shear strength tests

Abstract

Recently developed Cu@Ag nanoparticles render sintering process under air possible at low temperature for die attach application in power electronics devices. The development of Cu@Ag nanoparticles aims to decrease the cost of sintering nanopastes usually composed of pure silver nanoparticles. In this study, specific formulations of highly concentrated Cu@Ag nanoparticles based pastes were developed and their densification behavior was studied through dilatometry. The addition of a 6 nm silver shell around copper nanoparticles leads to a decrease of the densification temperature by almost 80°C. The achievement of highly densified metallic joints by hot pressing was fully characterized and demonstrated. Shear strengths above 20 MPa were measured after sintering under air at 200°C. Under inert atmosphere at 285°C, values up to 58 MPa were reached. These results demonstrate that Cu@Ag based nanopastes appear as a promising alternative to the common nano-silver based products for the production of high performance metallic joints.

1. Introduction

The growing need for "high temperature" power electronics modules requires the use of thermally resistant materials [1–3]. The assembly of chips onto substrates has been performed for years through sintering of silver pastes. These materials have gradually replaced traditional Pb or Sn-based soldering materials which are now considered either toxic or not enough resistant to heat [4]. At the nanometric scale, alteration of metal physical properties results in a decrease of the minimal temperature for sintering based densification [5]. The use of pastes based on silver nanoparticles (NPs) has been a breakthrough in lowering the densification temperature [6], typically between 200 and 300°C, to obtain joints with low porosity and high mechanical strength [7]. Furthermore, metallic joints issued from NPs sintering show thermal conductivity between 100 and 200 W/m.K, *i.e.* much higher than solder alloys [8]. However, the cost of silver remains a hurdle to use these solutions for most applications. A possible cost-driven advance would be to substitute silver with copper. Silver and copper hold very close thermal and electrical conductivities (~6% difference), and copper is a hundred times cheaper than silver. However, several barriers hinder ~~a priori~~ the use of copper such as its proneness to oxidation coupled with lower diffusion properties compared to silver [9]. The use

of pastes loaded only with copper NPs requires assembly stage to be carried out under inert or reducing atmospheres [10,11]. The need for such atmospheres hampers the transfer of these solutions to industry. To tackle these two problems, a proposed solution is to stabilize the Cu NPs through encapsulation. Several materials such as organic molecules [12], polymers [13] and metals [14,15] proved efficient to stabilize Cu NPs. The best route reported so far to prevent oxidation and to enhance densification is the encapsulation with silver [16,17]. However, this silver layer is only stable up to a certain temperature due to a dewetting phenomenon and a natural trend for Ag atoms to diffuse to the pores at the beginning of the sintering phase.[18,19] In a previous paper, we demonstrated that synthetized Cu@Ag NPs resist to oxidation up to 206°C under air when covered with a 6 nm silver shell [20].

From an applicative point of view for power electronics assembly, it appears necessary to incorporate NPs into a dedicated screen-printing formulation, with an appropriate viscosity [21]. Sintering pastes need to be highly concentrated in NPs to reach high densities. Formulations usually contain solvents, surfactants and other additives [22]. The main technique for evaluating the quality of a metallic joint is to evaluate its mechanical resistance through shear test. Densified silver joints show fracture values in the range of 10 to 60 MPa [23]. The mechanical strength is directly related to the final density; low porosities joints showing higher shear values [24–26].

In this study, Cu@Ag core-shell NPs were formulated in screen-printing nanopastes. Densification during free and pressure-assisted sintering was characterized and compared to a nano-silver commercial paste. Densification was predicted by calculation with and without pressure. The mechanical performances of Cu@Ag based nanopastes were then measured after hot pressing under air and nitrogen and correlated to microstructure analysis by SEM.

2. Materials and methods

2.1. Materials

Ethanol (96%), α-terpineol (≥ 96%), diethylene glycol monobutyl ether (noted DEB mbe, ≥ 98%), polyvinylpyrrolidone (noted PVP, 29000 $g.mol^{-1}$), polyethylene glycol (noted PEG, 200 $g.mol^{-1}$), L-ascorbic acid (noted AA, reagent grade) and formic acid (noted AF, ≥ 95%) were purchased from Sigma-Aldrich. Silver nanopaste Argomax 5020, developed for copper surfaces, was purchased from Alpha Assembly. Oxygen free high conductivity (OFHC) copper substrates of 24x17x3 mm^3 and dies of 5x5x3 mm^3 were purchased from Isomeca; without metallization layer.

2.2. Preparation of nanopastes and deposition process

Cu-PVP and Cu@Ag NPs were obtained via a polyol synthesis, galvanic displacement and post-treatments as described previously [20]. The spherical shaped core-shell nanoparticles obtained in a 5L reactor had a core diameter of 81±35 nm and a silver shell thickness of 6±3 nm. The core-shell NPs with a copper:silver molar ratio of 2.5:1 were washed by centrifugation in ethanol. The organic components were added to the suspension and the resulting dispersion was homogenized in a Turbula shaker-mixer. The pastes were concentrated by removing ethanol in a rotary evaporator. Cu@Ag NPs were formulated to obtain solutions for Cu to Cu die attach processing, as presented in Table 1. Carboxylic acids are added into the formulations to remove copper oxide without corroding copper surface atoms. In the Cu@Ag PEG paste, the polymer concentration is higher. It was decided to increase its concentration because of its ability to replace the solvents due to its similar viscosity at ambient temperature. Furthermore, it was proven that thermal decomposition of PEG occurs at low temperature and leads to carboxylic acids compounds [27,28]. Nanopastes, listed in Table 1, were then deposited with a manual screen-printing device (100 µm thick apertures) on degreased and deoxidized copper plates. The first paste in ethylene glycol was used for dilatometric tests and microstructure observation. For a statistical analysis of the shear strength after hot pressing, four deposits were carried out on each copper substrate of 24x17x3 mm^3. Four OFHC copper plates of 5x5x3 mm^3 were manually placed over the deposits to obtain Cu/Cu assemblies (Fig. 1) with similar sintering conditions to calculate an averaged shear stress value and the associated standard deviation. For dilatometric tests, the preparation was the same, except that the Cu/Cu assemblies were performed between two OFHC copper plates of 5x5x3 mm^3.

Table 1. Cu@Ag nanopastes compositions

Paste name	*Cu@Ag NPs (wt%)*	*Ethylene glycol (wt%)*	*α-terpineol (wt%)*	*DEG MBE (wt%)*	*PEG (wt%)*	*Additive (wt%)*
Cu@Ag	*80*	*20*	*-*	*-*	*-*	*-*
Cu@Ag AA	*80*	*-*	*15*	*2*	*1*	*Ascorbic acid 2*
Cu@Ag AF	*82*	*-*	*13.5*	*2*	*1.5*	*Formic acid 1*
Cu@Ag PEG	*85*	*-*	*5*	*-*	*10*	*-*
Cu-PVP	*75*	*25*	*-*	*-*	*-*	*-*

2.3. Instrumentations for densification study, assembly and shear tests

Densification of metallic joints was followed with a Setaram TMA 92 dilatometer under argon at a 12°C/min heating rate. The dilatometric tests were performed with a stack of two OFHC copper plates of 5x5x3 mm^3 assembled with Ag, Cu or Cu@Ag nanopastes, as explained in the previous section. Initially the load applied to the stack was set at 5 g (2 kPa). In a second step, in order to study the impact of uniaxial stress on densification, a load of 350 g (140 kPa) was applied. ~~Before sintering the joints, the deposits were debinded in an oven at 100°C for 30 min under air.~~ The deposits were debinded in an oven at 300 °C for 30 min in air, and immediately transferred to the heating press.

Hot pressing assemblies were performed using a Lauffer UVL heating press equipped with a primary vacuum pump. Fig. 1 shows a standard cycle for hot pressing sintering assemblies in air at 200°C for 30 min. The stress was applied gradually from the beginning of the cycle up to 10 MPa. The initial temperature was fixed at 50°C. The stress was applied until the end of the temperature drop. Hot pressing assemblies were also prepared under nitrogen at 285°C with the same profile, but with two cycles of vacuum (down to 10^3 Pa) before introducing nitrogen. Before hot pressing, deposits were debinded at 100°C during 30 min under air in an oven. The mechanical shear strength was measured with a bond tester (Nordson Dage 4000Plus), using a load cell of 200 kgf (1961 N). Joint microstructures were observed by SEM analysis on a LEO 1530 microscope from Zeiss. FIB preparations were performed with a FEI V600 and FIB 3D with a Dual Beam Zeiss Nvision. Image analysis was performed with FiJi (ImageJ) software.

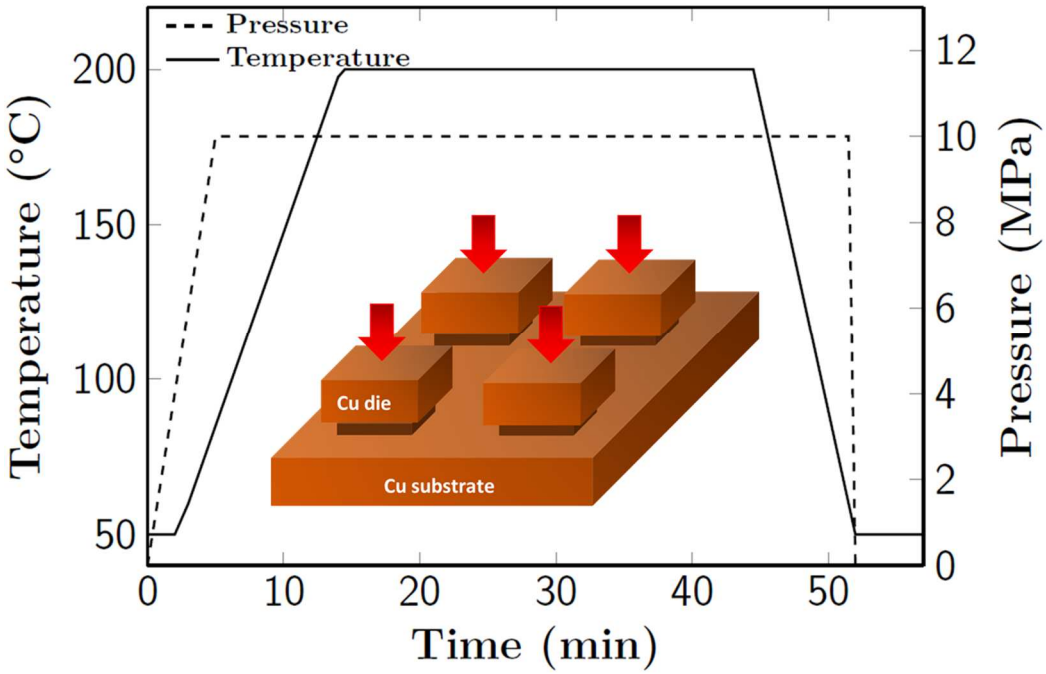

Fig. 1. Hot pressing sintering profile of Cu/paste/Cu assemblies.

3. Results and discussion

3.1. Dilatometric studies

Dilatometric tests were carried out to characterize the joint densification process for the Cu@Ag nanopaste formulated into ethylene glycol (first formulation in Table 1). This technique gives access to the thermal expansion measurement and, in the case of sintering, to the shrinkage caused by the densification process. It is thus possible to measure the densification of a powder or a paste, as a function of both time and temperature.

In a first step, three different pastes were compared: 1) the commercial silver paste Argomax 5020, 2) a copper paste formulated into ethylene glycol with 80 nm particle size Cu-PVP NPs (75wt%, noted Cu-PVP in Table 1) and 3) a Cu@Ag paste formulated into ethylene glycol with 85 nm particle size Cu@Ag NPs (80wt% noted Cu@Ag in Table 1) as listed in Table 1.

The initial weight density of the joint is the weight density of the paste and it is estimated by dividing the mass of deposited paste by the screen-printed volume (4x4x0.1 mm^3). The weight density of metallic material is deduced by multiplying by the fraction of non-organic material in the paste. Finally, the relative density D_i is obtained by dividing this value by the theoretical weight density of metallic material, which depends on its composition.

The temperature of the dilatometer chamber was raised to 500°C and then cooled down, without holding time and with a minimum uniaxial stress of 2 kPa. Fig. 2 a) displays values for the shrinkage, ΔL/L, and the variation of relative density during each test deduced from linear shrinkage measurement. The relative density was calculated with equation 1, according to constrained sintering, (*i.e.* without lateral deformation ΔL/L=ΔV/V):

$$D = \frac{Di}{1-\frac{\Delta L}{L_i}} \qquad (1)$$

where D is the relative density, D_i the initial density and $\frac{\Delta L}{L_i}$ the linear shrinkage.

Based on three samples, the average final relative density was calculated to be 0.66 for the Cu@Ag joint, 0.67 for the Ag joint and 0.57 for the Cu joint. ~~The most important information is certainly the onset temperature of sintering.~~ The most important information is certainly the onset temperature of sintering, which was determined by the inflexion point at which the relative density curves start rising. Densification begins at 250°C for the pure commercial silver paste and at 375°C for the pure copper paste. Interestingly, the addition of a silver shell significantly reduces the densification temperature of the system and the Cu@Ag NPs start to densify at only 300°C.

A second series of experiment was run. A pressure was then applied during the heating ramp to study the impact of stress on the variation of the relative density. The stresses usually applied during die attach processes were not achievable with our dilatometer. Nevertheless, it was possible to apply a 350 g load (140 kPa). Fig. 2 b) compares the stress effect on the variation of the relative density of joints following a cycle with a plateau at 300°C during 1 h under argon. One of the two assemblies was analyzed with a minimal stress of 2 kPa (5 g) as a reference. For the 2 kPa test, densification starts at the same temperature pointed out in Fig. 2 a), *i.e.* around 300°C. The final relative density is 0.31 which corresponds to an 11% relative increase ~~of only 0.03~~ (initial density is equal to 0.28). For the test carried out under 140 kPa stress, the temperature at the beginning of densification is lowered to 250°C, meaning that a stress of only 140 kPa is sufficient to lower the densification temperature by 50°C. The final relative density achieved in this case is 0.36 which corresponds to about 29% relative increase. ~~increase of 0.08~~. These two experiments show that, even for a fairly long plateau of 1 h at 300°C, low stresses lead to very low densification and that pressing clearly improves densification.

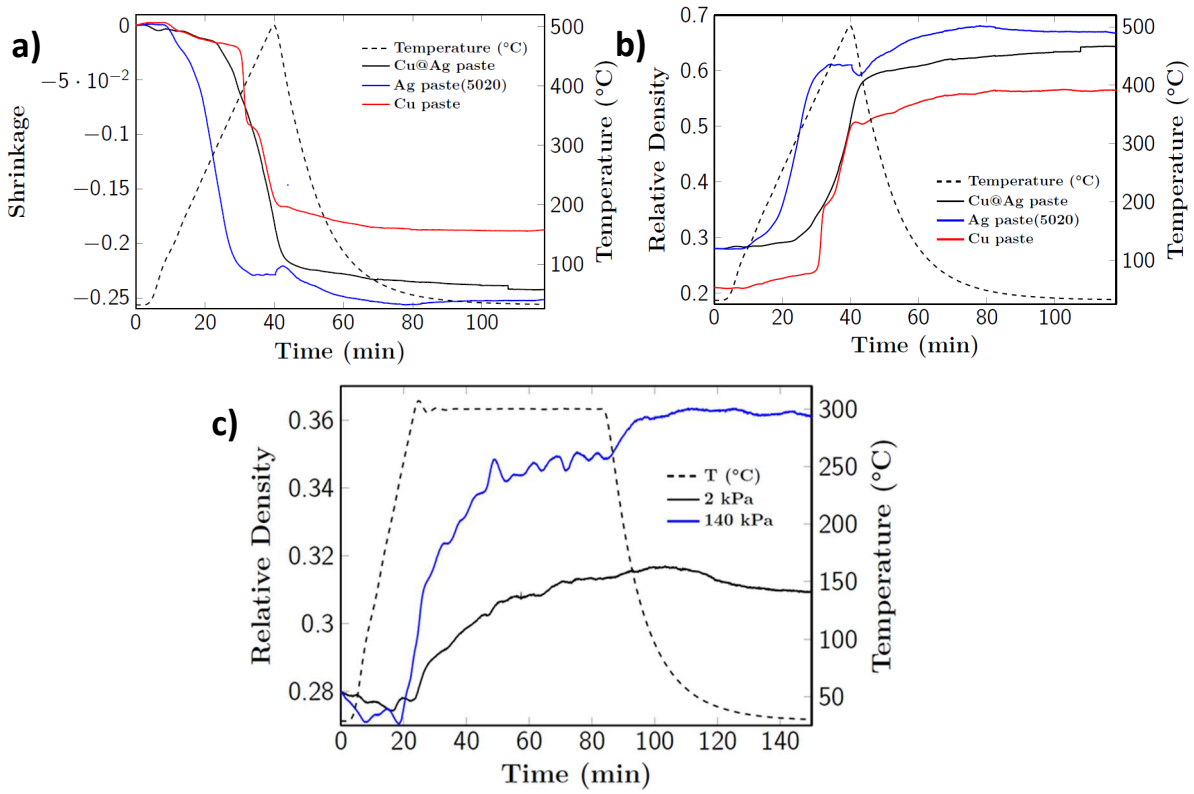

Fig. 2. a) Evolution of shrinkage and relative densities of Cu-PVP (noted Cu paste), Cu@Ag and Ag nanopastes with a temperature ramp up to 500°C under argon at 12°C/min and an applied stress of 2 kPa; b) Corresponding evolution of relative densities of Cu-PVP (noted Cu paste), Cu@Ag and Ag nanopastes with a temperature ramp up to 500°C under argon at 12°C/min and an applied stress of 2 kPa; c) Curves for Cu@Ag pastes under 140 kPa and 2 kPa during a 1 h plateau at 300°C under argon with a 12°C/min heating rate.

3.2. Microstructure after dilatometric tests

~~The Cu@Ag joint sintered at 500°C (Fig. 2 a)) was prepared with a Focused Ion Beam by excavation to observe its microstructure.~~ The microstructure of the Cu@Ag joint sintered at 500°C (Fig. 2a) was observed after preparation by a FIB. The cross-sectional view is shown in Fig. 3. The pores correspond to the darkest areas. Image analysis of the surface fraction indicates that the final porosity is 35%. This value is in good agreement with the value of 36% obtained by dilatometry (Fig. 2. c). Both other phases are identified from their density: bright areas correspond to the silver-rich phase (107.9 g/mol) whereas grey areas are ascribed to the copper-rich phase (63.5 g/mol). This is consistent with the elementary EDX ~~cartography~~ mapping where copper is displayed in red and silver in green (Fig. 3 b)). The approximate size of these Cu particles is in the order of several hundred nanometers.

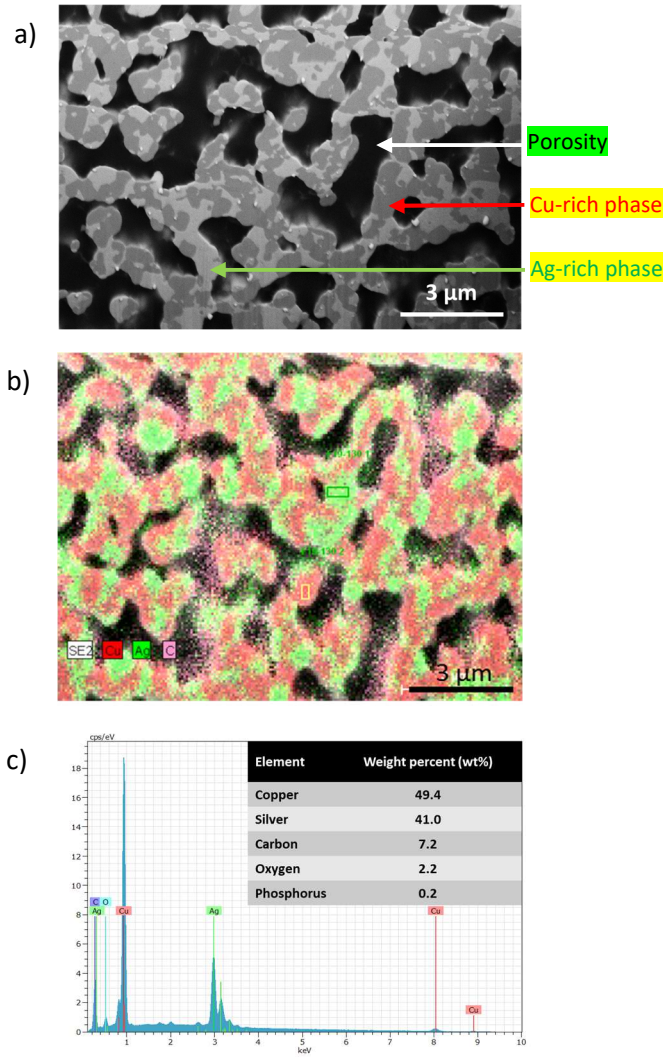

Fig. 3. a) SEM-BSE image of a Cu@Ag joint heated up-to 500°C, the sample was prepared by FIB, Cu-rich phase and Ag-Rich phase are identified by red and green arrows respectively, the black parts of the image correspond to pores; b) SEM-EDX elementary mapping (same area but with a slight vertical shift); c) EDX spectrum and associated element quantification.

3.3. Final density and microstructures after hot pressing

A new sample was sintered by hot pressing under 10 MPa during 30 min at 285°C under nitrogen atmosphere. Fig. 4 displays the final microstructure. The Cu@Ag nanopaste was identical to the one used for the dilatometric tests. ~~A 3D FIB characterization was performed with a stack of 340 SEM images acquired in the backscattered mode~~. The grey levels were assigned according to the chemical nature, based on the previous EDX analyses (Fig. 3). The dark areas represent the porosity, the green areas represent the Ag-rich zones and the red areas represent the Cu-rich zones. After watershed segmentation ~~(Fig. 4)~~, the copper grain size was evaluated from the Feret Diameter in the range 88-141 nm. The final porosity was estimated at 18%. Hot pressing leads to much higher relative densities than those obtained by dilatometry under low pressure.

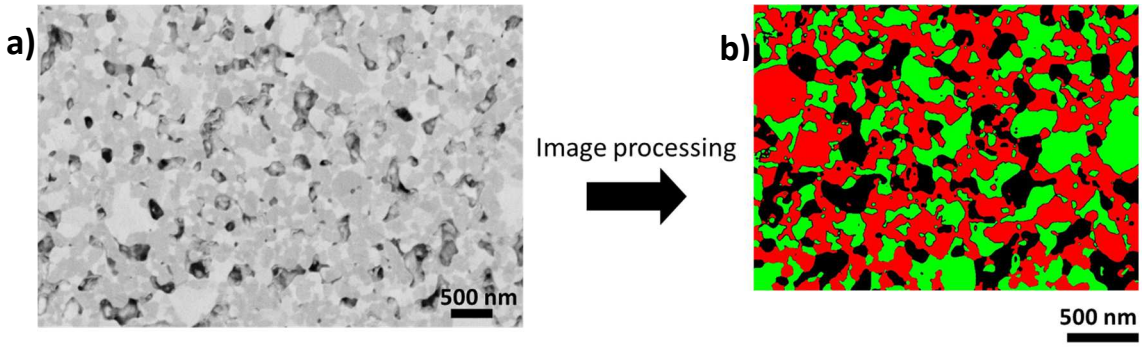

Fig. 4. a) SEM image of a Cu@Ag joint hot pressed for 30 min at 285°C under 10MPa; b) Image processing, colorization: Cu is represented in red, Ag in green and porosity in black.

The 3D reconstruction of the metal joint and its porosity network are shown in Fig. 5. SEM equipped with a focused ion beam (FIB-SEM) was used. After an observation box was dug by FIB, a 10 nm etching by ion beam was performed on the joint. A SEM image of the prepared zone was taken in the backscattered mode. Then the zone was etched again by 10 nm and this process was repeated 340 times. The recovered image stack was analyzed by image processing using FiJi (ImageJ) softwareThe metal part has a final relative density of more than 80%, so only the external surfaces are visible. The porosity network occupies less volume and therefore the 3D network is clearly visible.

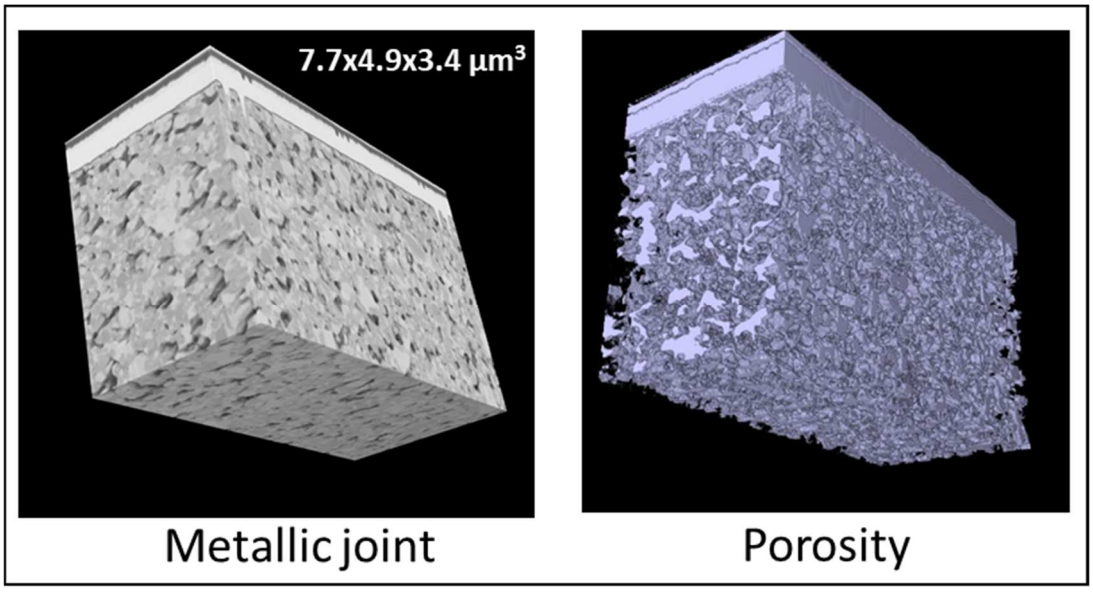

Fig. 5. 3D representations of a Cu@Ag metallic joint and its porosity after sintering during 10 min at 285°C under 10 MPa and N_2 atmosphere.

3.4. Densification modeling

Modeling of densification of a powder compact during sintering under uniaxial stress is complex. Various mechanisms may contribute to the pore elimination (particle rearrangement, atomic diffusion, viscoplastic deformation, etc) and many material parameters are involved. Evolution also strongly depends on the initial particle morphology and the packing microstructure. The situation is somewhat more complex for our Cu@Ag nanopastes due to the presence of organics, which may interfere with sintering and to the core-shell structure of nanoparticles in the paste. Therefore, a simplified approach is proposed hereinafter by adapting simple models from the literature to our system, in order to give rough estimates of densification kinetics.

A two-sphere model is used, with a core-shell structure for the particles (Fig. 6 a)). The central Cu sphere has a diameter of 80nm and the Ag layer has a thickness of 6 nm. Since mass transport to the pores essentially involves Ag atoms at the beginning, a further simplification is introduced by making calculation with plain Ag spheres for particle rapprochement below 2x6 nm and with plain Cu spheres for particle rapprochement above this value.

3.4.1. Dilatometric tests

Plastic deformation is assumed to play a minor role in the dilatometric experiments, since the applied stress remains far below the yield strength of Cu or Ag in the temperature range. Assuming that atomic diffusion is the main sintering mechanism, the classical two-sphere models of the literature can be applied. Grain boundary diffusion is usually the dominant mass transport path for ultrafine particles. Coble has expressed the neck growth kinetics for this mechanism by taking into account also the effect of the external uniaxial pressure applied on the powder compact [29–31]:

$$\left(\frac{X}{a}\right)^6 = \frac{96\delta_{GB}D_{GB}\Omega_a}{k_bTa^4}\left[\gamma + \frac{Pa}{\pi}\right].t \qquad (2)$$

where *X* is the neck radius (m), a is the particle radius (m), δ_{GB} is the grain boundary thickness (m), γ is the surface energy (J.m^{-2}), Ω_a is the atomic volume (m^3), k_b is the Boltzmann constant (J.K^{-1}); T is the temperature (K), *P* is the external pressure applied to the assembly (Pa), t is the time (s) and D_{GB} is the grain boundary diffusion coefficient expressed as:

$$D_{GB} = D_{GB0}.exp(-\frac{E_a}{RT}) \quad (3)$$

where D_{GB0} is the diffusion pre-exponential factor ($m^2.s^{-1}$), Ea is the activation energy ($J.mol^{-1}$), R is the gas constant ($J.K^{-1}.mol^{-1}$) and T is the temperature (K). The physical parameters used for the calculation are listed in Table 2.

Table 2. Parameters used for the calculation of X/a by grain boundary diffusion.

Parameter	*Symbol*	*Copper*	*Silver*
Grain boundary thickness (m)	δ_{GB}	*$5x10^{-10}$* [32,33]	
Grain boundary pre-exponential factor ($m^2.s^{-1}$)	D_{GB0}	*$1.65x10^{-7}$* [34]	*$3.00x10^{-6}$* [35]
Surface energy ($J.m^{-2}$)	γ	*1.8* [36]	*1.2* [36]
Atomic volume (m^3)	Ω	*$1.18x10^{-29}$* [33]	*$1.71x10^{-29}$* [32]
Activation energy ($J.mol^{-1}$)	E_a	*85300* [34]	*85000* [35]
Gas constant ($J.K^{-1}.mol^{-1}$)	R	*8.31*	
Boltzmann constant ($J.K^{-1}$)	k_b	*$1.38x10^{-23}$*	

Neck growth by atomic diffusion induces particle rapprochement and therefore linear shrinkage which can be related through the equation 4 [24]:

$$\frac{\Delta L}{L} = \frac{1}{4}\left(\frac{X}{a}\right)^2 \quad (4)$$

The relative density can be deduced from equation 1.

Fig. 6 b) presents the calculated relative density variation of Cu@Ag core-shell packings sintered at 200°C. The effect of the applied pressure of 0.140 MPa on sintering kinetics by atomic diffusion is negligible (Eq. 2). A value of 0.28 was taken for the initial relative density, as for the experimental Cu@Ag nanopaste. The density increase caused by silver sintering is 0.03 so that an intermediate density of 0.31 is reached after ~~20 s~~ 6 s. From ~~20 s~~ s 6 s onwards, the 80 nm copper NPs further densify the system ~~by 7%,~~ by 0.07 which corresponds to a 22 % relative increase, to reach a final density of 0.38 after 5 min. In the case of sintering at 200°C, without pressing, the final porosity is thus 62%. Fig. 6 c) presents the calculated relative density variation at 300°C, as in the dilatometric experiments (Fig. 2 b)). At 300°C, kinetics are much faster and final density values are reached after only 100 ms. The calculated density values are the same at 300°C as in the dilatometric experiments (Fig. 2 b)) as shown in the Fig. 6 c). At 0 MPa, the value is in agreement with dilatometry and microstructural analyses after sintering with very low stresses (see Fig. 2 b) and Fig. 3 a)). The much stronger densification observed experimentally with 140 kPa stress (Fig. 2 b)) is probably due to particle rearrangement, often observed during sintering of low density packings. This particle

rearrangement is not taken into account by the neck growth model. Anyhow, the porosity value after sintering at 300°C under low uniaxial stress is too high for providing a mechanically resistant joint.

3.4.2. Hot pressing experiments

The high pressure applied during the hot pressing of joints for chip transfer involves plastic deformation in addition to diffusion. In a first approach, only the instantaneous plastic deformation occurring at room temperature has been calculated. A complete model should include the viscoplastic deformation taking place during the whole heating cycle, which would need further assumptions and the introduction of the temperature dependence of physical parameters. The present approach then underestimates the contribution of plasticity to densification.

Plastic deformation of NPs occurs when the effective pressure (P_{eff}) at interparticle contacts is greater than three times the elastic limit of the material ($P_{eff} \geq 3\sigma_y$). The effective pressure can be approximated by equation 5 [37].

$$P_{eff} = \frac{P(1-D_i)}{D^2(D-D_i)} \quad (5)$$

where P is the external pressure applied to the assembly (Pa), D_i is the initial relative density and D the instantaneous relative density.

For an applied external pressure of 10 MPa, the effective pressure at interparticle contacts is in the order of several GPa. In the case of Cu@Ag NPs, the yield strength is approximated at 50 MPa for both copper and silver metals at ambient temperature [37,38]. The effective pressure is much higher than $3\sigma_y$. A simplified calculation of densification by plastic deformation is then given by the following relationship (Equation 6) [37]:

$$D_{yield} = \left(\frac{(1-D_i)P}{1.3\sigma_y} + D_i^3\right)^{\frac{1}{3}} \quad (6)$$

where σ_y is the yield strength of the material (Pa).

Taking an initial paste density of 0.28, with a yield strength value of 50 MPa, the calculation gives a relative density of 0.51 after plastic deformation. Once densification during the compaction step at ambient temperature has been estimated, the densification during heating is calculated by taking into account atomic diffusion only, as mentioned previously. The effect of the applied pressure of 10 MPa on sintering kinetics by atomic diffusion is still negligible (Eq. 2). Fig. 6 b) shows the densification calculated for the Cu@Ag system, under uniaxial stress of 10 MPa at 200°C. Silver diffusion increases the density from 0.51 to 0.56 after 2 s. Subsequently, the diffusion of copper

results in a maximum relative density of 0.76 after 5 min. At 300°C densification kinetics are higher but density values are similar. This last calculated value of 0.76 is consistent with the measured value of 0.82 (see Fig. 4). The contribution of stress is thus significant in the calculation and allows obtaining much higher final densities. This can be explained both by the significant densification during cold compaction and by the higher contribution of sintering shrinkage to the densification, starting with a higher green density (see Eq. 1). It should be reminded that the model does not take into account the viscoplastic deformation during heating. For example, by applying Eq. 6 with the final density value of 0.76, back to ambient temperature, the plastic deformation would densify up to a relative density of 0.78.

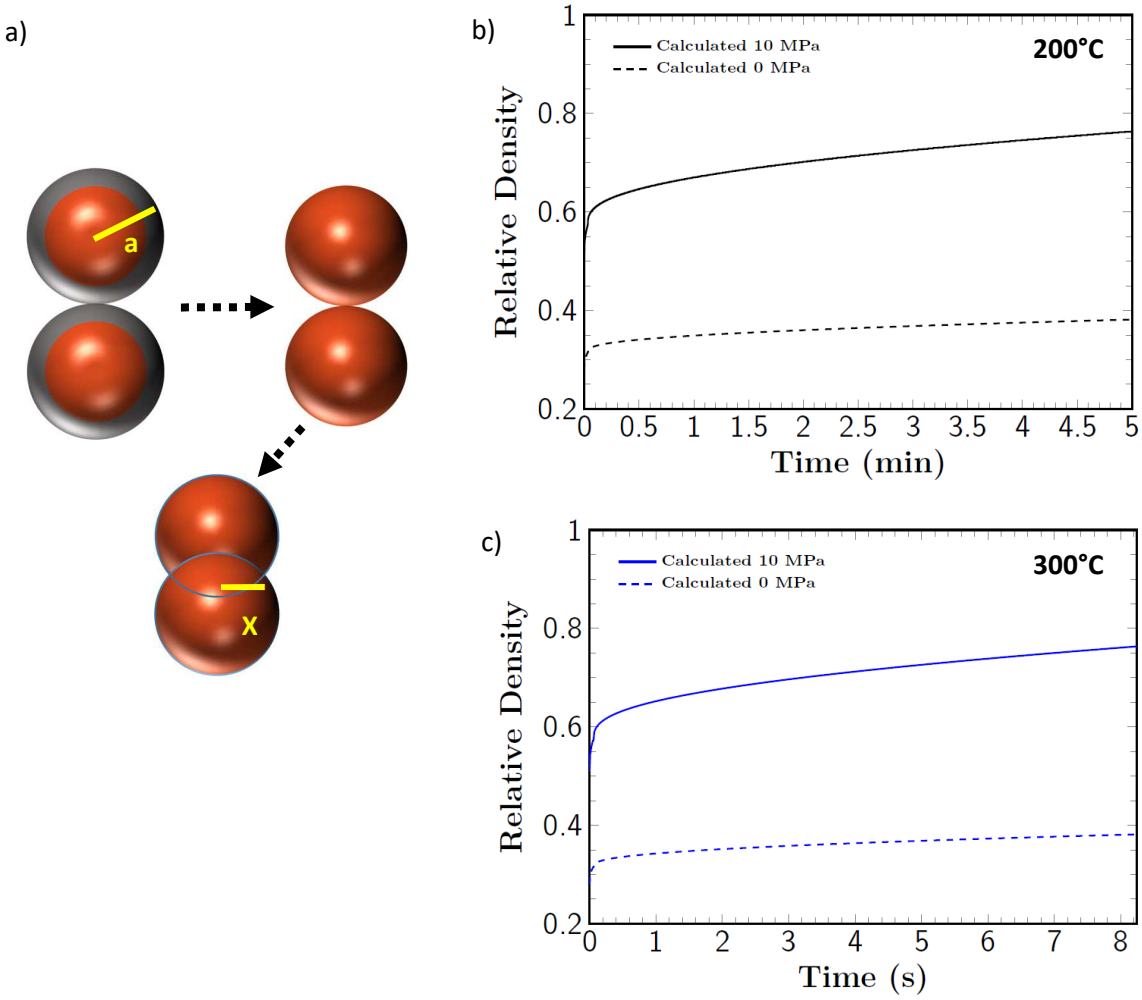

Fig. 6. a) Scheme of two core-shell Cu@Ag NPs before silver diffusion and two Cu NPs before copper diffusion; b) Densification model of Cu (80 nm) Ag (92 nm) NPs by calculation with a model of grain boundary diffusion at 200°C without external stress and with a 10 MPa stress; c) Densification model of Cu (80 nm) Ag (92 nm) NPs by calculation with a model of grain boundary diffusion at 300°C without external stress and with a 10 MPa stress.

3.5. Mechanical strength of sintered Cu@Ag joints after hot pressing at 10 MPa

Cu/Cu hot pressed junctions were mechanically tested. Picture in Fig. 7 a) shows the fracture morphology of a Cu@Ag joint after being mechanically tested, a slight deformation of the metal grains on the surface is noticeable. Fig. 7 b) shows shear results for joints sintered in air at 200°C. The reference silver joint has a shear srength of 11 ± 6 MPa when sintered for 30 min. The value reached after a sintering time of 60 min slightly decreases to 10 ± 2 MPa. None of the two values exceeds the minimum required threshold of 12 MPa (MIL-STD-883 standard [39]) in these conditions. Ag Argomax 5020 is marketed for sintering from 200°C to 300°C on copper surfaces under air. The rather low values observed for this reference may be ascribed to the slight oxidation of the copper substrates during the assembly cycles. For the Cu@Ag formulated nanopastes, no lead exceeding 12 MPa was noted after a sintering time of 30 min. With a 60 min hold at 200°C, the three Cu@Ag metal joints overcome the standard minimum value. In the case of the highly concentrated formulation in PEG, a)
Cu@Ag PEG, the value is 19 ± 5 MPa. In the presence of formic acid, Cu@Ag AF, the rupture occurs at 15 ± 6 MPa. The best value is obtained for a sintered joint with a Cu@Ag paste containing ascorbic acid, Cu@Ag AA: the joint breaks at 21 ± 2 MPa. Thus, it appears that Cu@Ag joints are promising solutions compared to Ag joints for low temperature air sintering on copper surfaces. This is certainly due to the presence of copper, which is prone to create stronger bonds with substrates than pure silver.

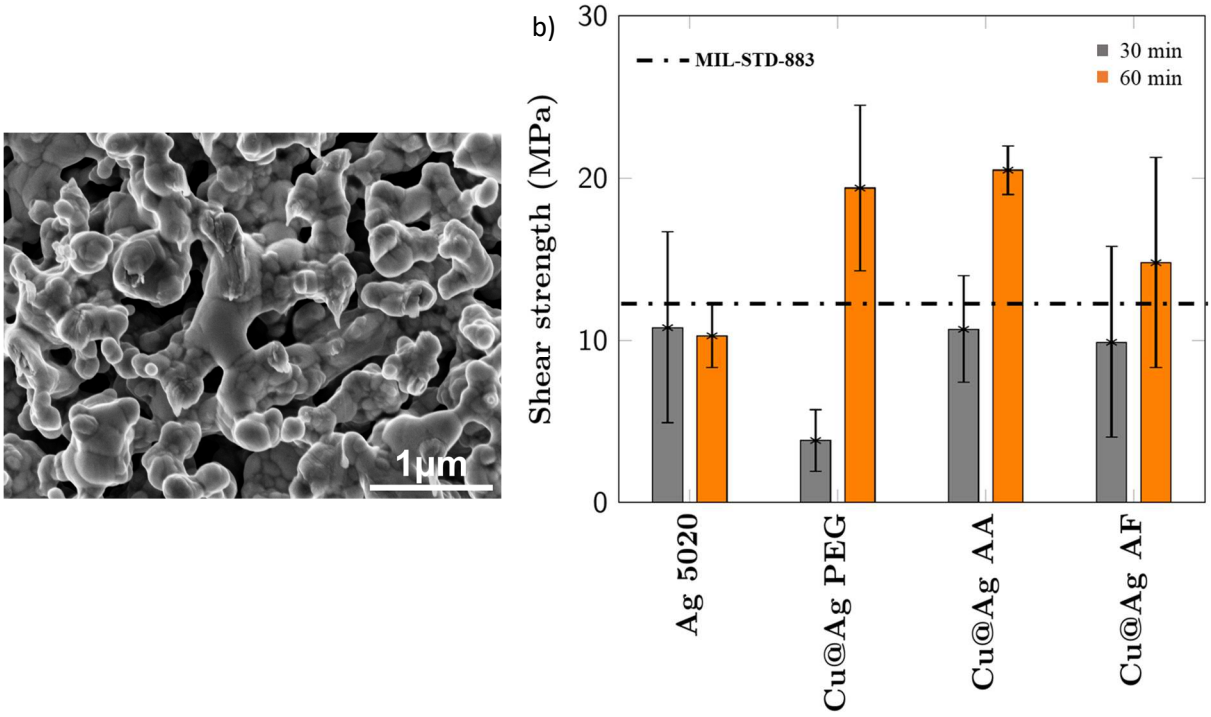

Fig. 7. a) SEM Image of fracture morphology of a sintered Cu@Ag joint after shear test; b) Shear strength of Ag and Cu@Ag joints after two sintering durations at 200°C-10 MPa in air. The minimum limit imposed by the MIL-STD-883J is indicated by the black dashed line for sake of clarity.

Under nitrogen, at 285°C the obtained shear values are much higher than those obtained at 200°C. Fig. 8 shows histograms of the values obtained for the same four metal joints as above. After only 10 min, all shear strengths exceed 20 MPa. At 10 min (blue bars), the Ag reference joint appears to be the most resistant, with a rupture value measured at 45 ± 13 MPa. For Cu@Ag joints, PEG and ascorbic acid formulations break at almost the same value, *i.e.* 33 ± 5 MPa and 32 ± 6 MPa respectively. The less resistant joint comes from the formulation containing formic acid with a final value of 25 ± 6 MPa. After only 10 min of sintering at 285°C, all joints show shear strengths well above 12 MPa. These results also show that pure Ag NPs sinter faster than Cu@Ag NPs.

After 20 min, the Cu@Ag formulation with ascorbic acid leads to a value of 53 ± 5 MPa. Then the Ag joint breaks at 47 ± 5 MPa and the Cu@Ag joint from the PEG formulation breaks at 40 ± 3 MPa. The formic acid formulation gives surprisingly a lower value with a rupture figure of 22 ± 2 MPa.

For the assembly series with a 30 min plateau, the order of values is similar. The Cu@Ag system sintered in the presence of ascorbic acid breaks has the highest recorded shear strength value, topping 58 ± 4 MPa. This is the best value obtained for all joints sintered under our experimented conditions. The Ag joint reaches 54 ± 8 MPa, while the other two Cu@Ag joints reach 44 ± 8 MPa for

the PEG formulation and 42 ± 10 MPa for the formic acid formulation. These values are remarkably high, ranking the Cu@Ag joints among the most resistant metal joints reported so far.

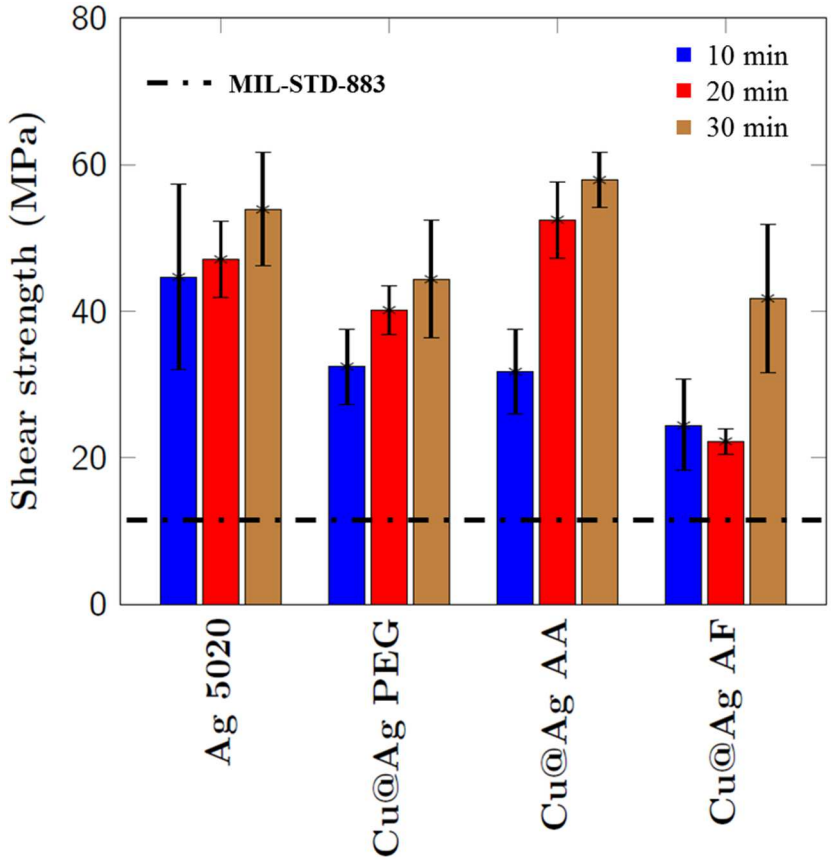

Fig. 8. Shear strength of Ag and CuAg joints at different sintering durations under 285°C-10 MPa and N_2 atmosphere. The minimum limit imposed by the MIL-STD-883J is indicated by the black dashed line for sake of clarity.

Several shear strength values from the literature are plotted in Figure 9. The two best results of our study with Cu@Ag joints are represented by the green star for the sample obtained after sintering at 200°C (60 min/10 MPa/Air) and by the purple star for the best result obtained after sintering at 285°C (30 min/10 MPa/N_2).

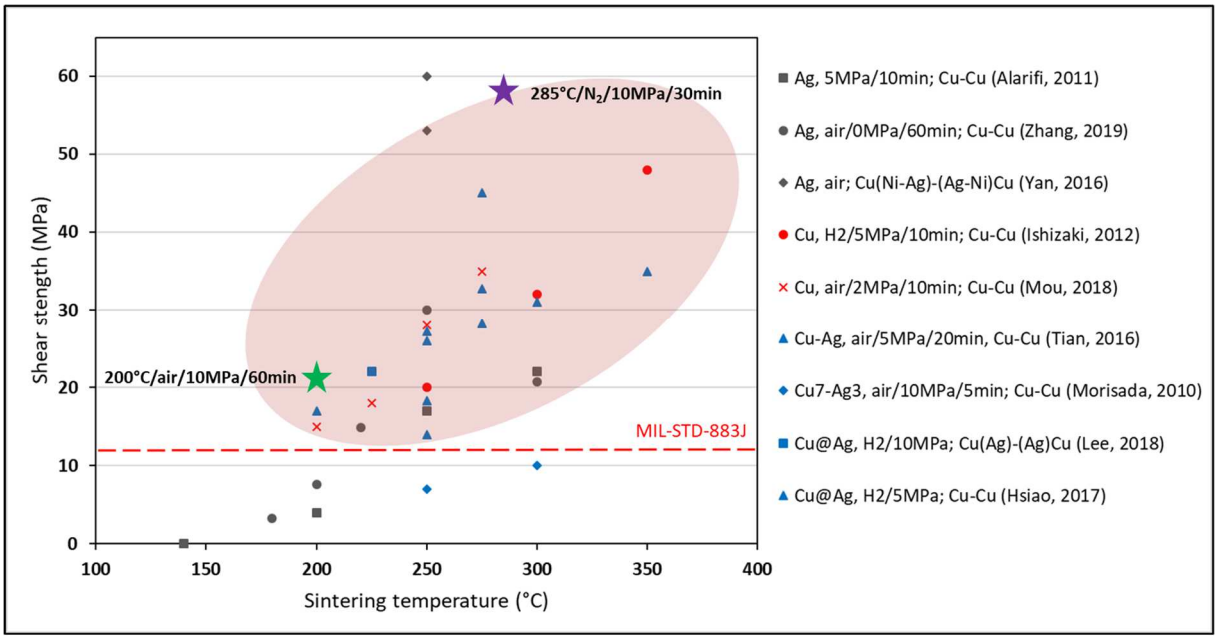

Fig. 9. Comparison of various shear strength values of metal joints extracted from the literature. Green and purple stars are related to the Cu@Ag sintered joints of the present study. Sintering conditions and metallic assembled surfaces are given for each plot [10,11,17,23,40–44]. The limit imposed by the MIL-STD-883J is indicated by the red dashed line for sake of clarity.

4. Discussion

The densification of the paste with Cu@Ag core-shell nanoparticles during free sintering or sintering under low applied stress and below 300°C is very limited. The green density is about 28% and the sintered density remains below 36% according to the dilatometric study (Figure 2). This is consistent with the model assuming atomic diffusion as the main densification mechanism (Figure 6). Indeed, even if neck growth by atomic diffusion were completed, with a relative neck size x/a = 1, the linear shrinkage would be around 25% from Eq. (4) and the final density would only be 37% from Eq. (1) due to the anisotropic shrinkage. Actually, with a structure as open as a nanopaste, particle rearrangement is needed in addition to neck growth for efficient densification. This can be visualized in the microstructure of Figure 3 where it is clear that deformation of particle chains is necessary to get further densification. Temperature can play a role but essentially it is the applied pressure which can efficiently reorganize the particle packing. With a simple model of powder compaction at room temperature, we have shown that the effect of pressure was the main contribution to densification of the paste sintered at 200 or 300°C (Figure 6). The viscoplastic deformation during heating should be modelled to get a full representation of densification during hot pressing, but the basic model already shows the right trend and it is consistent with the density of 82% measured after hot

pressing at 300°C. As for the practical aspects, hot pressing is then the most efficient way to densify the Cu@Ag paste below 300°C, a temperature which cannot be overpassed without damaging the electronic components.

5. Conclusion

In this work, we report that the sintering of Cu@Ag NPs shows much faster diffusion kinetics compared to simple copper nanoparticles. Dilatometric densification analyses have revealed that the Cu@Ag system begins to densify at around 300°C without stress. This temperature is much lower than the 375°C observed for sintering Cu-PVP nanoparticles. This decrease in the densification temperature is explained by the faster atomic diffusion in the silver layer present around copper nanoparticles. The addition of a low stress during these tests further decreases the densification temperature down to 250°C and allows higher densification (3% at 2 kPa versus 8% at 140 kPa at 300°C). Under very low stress (2 kPa), the sintering analyses have shown that grain growth is favored with sizes of several hundreds of nm, whereas hot pressing results in grain sizes limited to one hundred of nm. The relative densities obtained under very low stress are very low and do not exceed 0.4 whereas with high stress (10 MPa) the density can reach values higher than 0.8. These data are in agreement with the ones predicted by a densification model taking into account copper and silver atomic diffusion and plastic deformation during compaction at room temperature. Cu@Ag formulated nanopastes lead to mechanical performances equal to those of commercial nano-Ag pastes. These results show that these core-shell NPs, with a silver thickness of 6 nm, appear as a promising alternative for power assembly sintering since Cu@Ag joints are mechanically more efficient on copper surfaces than reference Ag joints when hot pressed at 200°C under 10 MPa. Under air, Cu@Ag nanopaste with ascorbic acid reaches a mechanical resistance up to 21 MPa. For a higher assembly temperature of 285°C under nitrogen, Cu@Ag formulations require longer processing durations to obtain very high mechanical resistances, *i.e.* 58 MPa. The results of this work demonstrate that Cu@Ag NPs, with 6 nm thick silver shells and formulated with selected organic compounds, pave the way for an innovative and efficient solution for die attach process.

Declaration of Competing Interest

The authors declare that they have no known competing financial interests or personal relationships that could have appeared to influence the work reported in this paper.

Acknowledgment

The authors are grateful to B. Chemineau for FIB preparations and N. Botter for help in dilatometry experiments.

References

[1] C.B. O'Neal, B. McGee, B. McPherson, J. Stabach, R. Lollar, R. Liederbach, B. Passmore, Advanced Materials for High Temperature, High Performance, Wide Bandgap Power Modules, J. Electron. Mater. 45 (2016) 245–254. https://doi.org/10.1007/s11664-015-4187-5.

[2] C. Buttay, D. Planson, B. Allard, D. Bergogne, P. Bevilacqua, C. Joubert, M. Lazar, C. Martin, H. Morel, D. Tournier, C. Raynaud, State of the art of high temperature power electronics, Mater. Sci. Eng. B Solid-State Mater. Adv. Technol. 176 (2011) 283–288. https://doi.org/10.1016/j.mseb.2010.10.003.

[3] A. Hu, J. Janczak-Rusch, T. Sano, Joining Technology Innovations at the Macro, Micro, and Nano Levels, Appl. Sci. 9 (2019) 3568. https://doi.org/10.3390/app9173568.

[4] V.R. Manikam, K.Y. Cheong, Die attach materials for high temperature applications: A review, IEEE Trans. Compon. Packag. Manuf. Technol. 1 (2011) 457–478. https://doi.org/10.1109/TCPMT.2010.2100432.

[5] Y. Adda, J. Philibert, La diffusion dans les solides Tome II, Bibliothèque des Sciences et Techniques Nucléaires, 1966.

[6] H. Schwarzbauer, R. Kuhnert, Novel Large Area Joining Technique for Improved Power Device Performance, IEEE Trans. Ind. Appl. 27 (1991) 93–95. https://doi.org/10.1109/28.67536.

[7] K.S. Siow, Are sintered silver joints ready for use as interconnect material in microelectronic packaging?, J. Electron. Mater. 43 (2014) 947–961. https://doi.org/10.1007/s11664-013-2967-3.

[8] K.S. Tan, Y.H. Wong, K.Y. Cheong, Thermal characteristic of sintered Ag-Cu nanopaste for high-temperature die-attach application, Int. J. Therm. Sci. 87 (2015) 169–177. https://doi.org/10.1016/j.ijthermalsci.2014.08.022.

[9] Y. Mou, Y. Peng, Y. Zhang, H. Cheng, M. Chen, Cu-Cu bonding enhancement at low temperature by using carboxylic acid surface-modified Cu nanoparticles, Mater. Lett. 227 (2018) 179–183. https://doi.org/10.1016/j.matlet.2018.05.037.

[10] T. Ishizaki, R. Watanabe, A new one-pot method for the synthesis of Cu nanoparticles for low temperature bonding, J. Mater. Chem. 22 (2012) 25198–25206. https://doi.org/10.1039/c2jm34954j.

[11] C.-H. Hsiao, W.-T. Kung, J.-M. Song, J.-Y. Chang, T.-C. Chang, Development of Cu-Ag pastes for high temperature sustainable bonding, Mater. Sci. Eng. A. 684 (2017) 500–509. https://doi.org/10.1016/j.msea.2016.12.084.

[12] M.A. Ben Aissa, B. Tremblay, A. Andrieux-Ledier, E. Maisonhaute, N. Raouafi, A. Courty, Copper nanoparticles of well-controlled size and shape: a new advance in synthesis and self-organization, Nanoscale. 7 (2015) 3189–3195. https://doi.org/10.1039/C4NR06893A.

[13] Y. Jianfeng, Z. Guisheng, H. Anming, Y.N. Zhou, Preparation of PVP coated Cu NPs and the application for low-temperature bonding, J. Mater. Chem. 21 (2011) 15981–15986. https://doi.org/10.1039/c1jm12108a.

[14] T.G. Kim, H.J. Park, K. Woo, S. Jeong, Y. Choi, S.Y. Lee, Enhanced Oxidation-Resistant Cu@Ni Core-Shell Nanoparticles for Printed Flexible Electrodes, ACS Appl. Mater. Interfaces. 10 (2018) 1059–1066. https://doi.org/10.1021/acsami.7b14572.

[15] X. Liu, S. He, H. Nishikawa, Low temperature solid-state bonding using Sn-coated Cu particles for high temperature die attach, J. Alloys Compd. 695 (2017) 2165–2172. https://doi.org/10.1016/j.jallcom.2016.11.064.

[16] M. Grouchko, A. Kamyshny, S. Magdassi, Formation of air-stable copper-silver core-shell nanoparticles for inkjet printing, J. Mater. Chem. 19 (2009) 3057–3062. https://doi.org/10.1039/b821327e.
[17] Y. Tian, Z. Jiang, C. Wang, S. Ding, J. Wen, Z. Liu, C. Wang, Sintering mechanism of the Cu-Ag core-shell nanoparticle paste at low temperature in ambient air, RSC Adv. 6 (2016) 91783–91790. https://doi.org/10.1039/C6RA16474A.
[18] D. Bridges, C. Ma, Z. Palmer, S. Wang, Z. Feng, A. Hu, Laser brazing of Inconel® 718 using Ag and Cu-Ag nanopastes as brazing materials, J. Mater. Process. Technol. 249 (2017) 313–324. https://doi.org/10.1016/j.jmatprotec.2017.06.010.
[19] C. Ma, S. Xue, D. Bridges, Z. Palmer, Z. Feng, A. Hu, Low temperature brazing nickel with Ag nanoparticle and Cu-Ag core-shell nanowire nanopastes, J. Alloys Compd. 721 (2017). https://doi.org/10.1016/j.jallcom.2017.06.016.
[20] T. Michaud, S.S. Nobre, T. Baffie, N. Pelissier, J.-P. Simonato, High-temperature stability of copper nanoparticles through Cu@Ag nanostructures, J. Nanoparticle Res. 21 (2019). https://doi.org/10.1007/s11051-019-4567-5.
[21] M.J. Kammer, A. Muza, J. Snyder, A. Rae, S.J. Kim, C.A. Handwerker, Optimization of Cu-Ag Core-Shell Solderless Interconnect Paste Technology, IEEE Trans. Compon. Packag. Manuf. Technol. 5 (2015) 910–920. https://doi.org/10.1109/TCPMT.2015.2438816.
[22] J.G. Bai, J.N. Calata, G.-Q. Lu, Processing and characterization of nanosilver pastes for die-attaching SiC devices, IEEE Trans. Electron. Packag. Manuf. 30 (2007) 241–245. https://doi.org/10.1109/TEPM.2007.906508.
[23] J. Yan, D. Zhang, G. Zou, L. Liu, H. Bai, A. Wu, Y.N. Zhou, Sintering Bonding Process with Ag Nanoparticle Paste and Joint Properties in High Temperature Environment, J. Nanomater. 2016 (2016). https://doi.org/10.1155/2016/5284048.
[24] J. Li, C.M. Johnson, C. Buttay, W. Sabbah, S. Azzopardi, Bonding strength of multiple SiC die attachment prepared by sintering of Ag nanoparticles, J. Mater. Process. Technol. 215 (2015) 299–308. https://doi.org/10.1016/j.jmatprotec.2014.08.002.
[25] M. Knoerr, A. Schletz, Power semiconductor joining through sintering of silver nanoparticles: Evaluation of influence of parameters time, temperature and pressure on density, strength and reliability, in: 2011. https://www.scopus.com/inward/record.uri?eid=2-s2.0-79953743999&partnerID=40&md5=6f8c44e2567b6b43826d2cce6194998f.
[26] R. Khazaka, B. Thollin, L. Mendizabal, D. Henry, R. Khazaka, R. Hanna, Characterization of nanosilver dry films for high-temperature applications, IEEE Trans. Device Mater. Reliab. 15 (2015) 149–155. https://doi.org/10.1109/TDMR.2015.2402294.
[27] J. Glastrup, Degradation of polyethylene glycol. A study of the reaction mechanism in a model molecule: Tetraethylene glycol, Polym. Degrad. Stab. 52 (1996) 217–222. https://doi.org/10.1016/0141-3910(95)00225-1.
[28] J.N. Hemenway, T.C. Carvalho, V.M. Rao, Y. Wu, J.K. Levons, A.S. Narang, S.R. Paruchuri, H.J. Stamato, S.A. Varia, Formation of reactive impurities in aqueous and neat polyethylene glycol 400 and effects of antioxidants and oxidation inducers, J. Pharm. Sci. 101 (2012) 3305–3318. https://doi.org/10.1002/jps.23198.
[29] R.L. Coble, Diffusion models for hot pressing with surface energy and pressure effects as driving forces, J. Appl. Phys. 41 (1970) 4798–4807. https://doi.org/10.1063/1.1658543.
[30] M.N. Khiat, X. Wang, L. Benabou, L. Chassagne, J. Linares, Modeling of the densification of silver particles during sintering at controlled pressure and temperature, in: 2018. https://doi.org/10.1088/1742-6596/1141/1/012157.
[31] M.N. Rahaman, Ceramic processing and sintering, second edition, 2017. https://doi.org/10.1201/9781315274126.
[32] T. Geoffroy, Assemblages électroniques par frittage d'argent pour équipements aéronautiques fonctionnant en environnements sévères, PhD Thesis, Paris Sciences et Lettres, 2017.

[33] C.L. Martin, L.C.R. Schneider, L. Olmos, D. Bouvard, Discrete element modeling of metallic powder sintering, Scr. Mater. 55 (2006) 425–428. https://doi.org/10.1016/j.scriptamat.2006.05.017.
[34] L. Klinger, Y. Amouyal, S.V. Divinski, E. Rabkin, Grain boundary diffusion in recrystallizing nanocrystalline materials, Defect Diffus. Forum. 289–292 (2009) 641–648. https://doi.org/10.4028/www.scientific.net/DDF.289-292.641.
[35] J. Kučera, Self-diffusion in polycrystalline silver, Czechoslov. J. Phys. 14 (1964) 915–922. https://doi.org/10.1007/BF01789066.
[36] L. Vitos, A.V. Ruban, H.L. Skriver, J. Kollár, The surface energy of metals, Surf. Sci. 411 (1998) 186–202.
[37] A.S. Helle, K.E. Easterling, M.F. Ashby, Hot-isostatic pressing diagrams: New developments, Acta Metall. 33 (1985) 2163–2174. https://doi.org/10.1016/0001-6160(85)90177-4.
[38] H.J. Frost, M.F. Ashby, Deformation-mechanism maps: the plasticity and creep of metals and ceramics, Pergamon Press, 1982. https://books.google.fr/books?id=s9BRAAAAMAAJ.
[39] D. of Defense, MIL-STD-883 Test method standard: microcircuits, n.d.
[40] H. Alarifi, A. Hu, M. Yavuz, Y.N. Zhou, Silver nanoparticle paste for low-temperature bonding of copper, J. Electron. Mater. 40 (2011) 1394–1402. https://doi.org/10.1007/s11664-011-1594-0.
[41] Z. Zhang, C. Chen, Y. Yang, H. Zhang, D. Kim, T. Sugahara, S. Nagao, K. Suganuma, Low-temperature and pressureless sinter joining of Cu with micron/submicron Ag particle paste in air, J. Alloys Compd. 780 (2019) 435–442. https://doi.org/10.1016/j.jallcom.2018.11.251.
[42] Y. Mou, H. Cheng, Y. Peng, M. Chen, Fabrication of reliable Cu-Cu joints by low temperature bonding isopropanol stabilized Cu nanoparticles in air, Mater. Lett. 229 (2018) 353–356. https://doi.org/10.1016/j.matlet.2018.07.061.
[43] Y. Morisada, T. Nagaoka, M. Fukusumi, Y. Kashiwagi, M. Yamamoto, M. Nakamoto, A low-temperature bonding process using mixed Cu-Ag nanoparticles, J. Electron. Mater. 39 (2010) 1283–1288. https://doi.org/10.1007/s11664-010-1195-3.
[44] C.H. Lee, E.B. Choi, J.-H. Lee, Characterization of novel high-speed die attachment method at 225 °C using submicrometer Ag-coated Cu particles, Scr. Mater. 150 (2018) 7–12. https://doi.org/10.1016/j.scriptamat.2018.02.029.

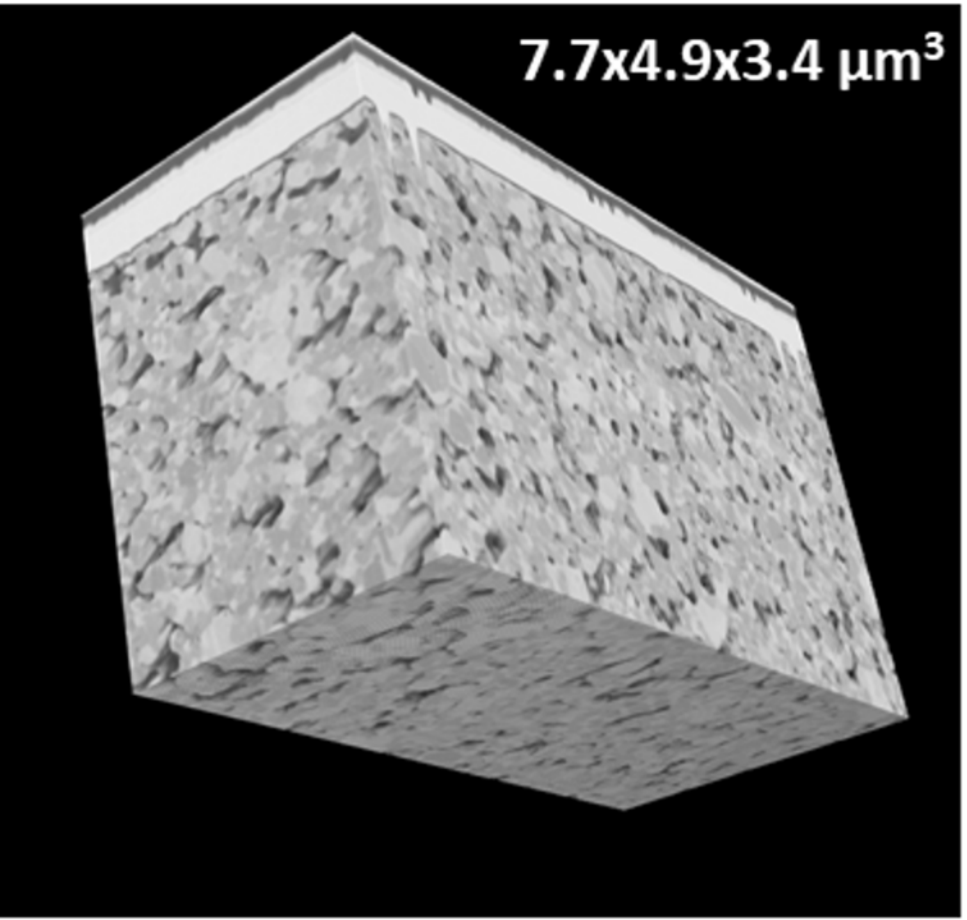

Metallic joint

Shear test

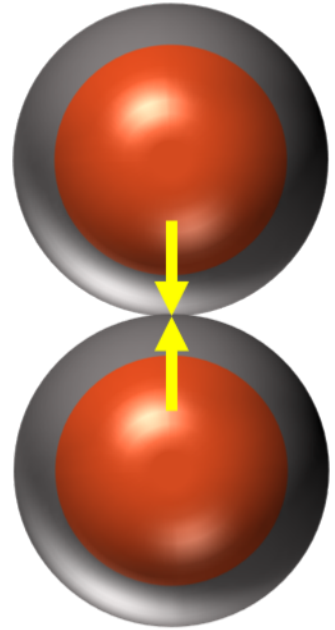

Cu@Ag NPs